Journal of Biomolecular NMR, 1 (1991) 323–347
ESCOM

J-Bio NMR 037

Solution structure of actinomycin–DNA complexes: Drug intercalation at isolated G-C sites

Xiucai Liu, Huifen Chen and Dinshaw J. Patel*

Department of Biochemistry and Molecular Biophysics, College of Physicians and Surgeons, Columbia University, New York, NY 10032, U.S.A.

Dedicated to the memory of Professor V.F. Bystrov

Received 18 July 1991
Accepted 12 August 1991

Keywords: Drug–DNA interaction; Actinomycin; Restrained molecular dynamics; Nuclear Overhauser effect; NOE; 2D NMR

SUMMARY

The actinomycin-D–d(A1-A2-A3-G4-C5-T6-T7-T8) complex (1 drug per duplex) has been generated in aqueous solution and its structure characterized by a combined application of two-dimensional NMR experiments and molecular dynamics calculations. We have assigned the exchangeable and nonexchangeable proton resonances of Act and d(A_3GCT_3) in the complex and identified the intermolecular proton-proton NOEs that define the alignment of the antitumor agent at its binding site on duplex DNA. The molecular dynamics calculations were guided by 70 intermolecular distance constraints between Act and nucleic acid protons in the complex. The phenoxazone chromophore of Act intercalates at the $(G\text{-}C)_I{\cdot}(G\text{-}C)_{II}$ step in the d(A_3GCT_3) duplex with the phenoxazone ring stacking selectively with the $G4_I$ and $G4_{II}$ purine bases but not with $C4_I$ and $C4_{II}$ pyrimidine bases at the intercalation site. There is a pronounced unwinding between the A3·T6 and G4·C5 base pairs which are the next steps located in either direction from the intercalation site in the Act–d(A_3GCT_3) complex. The Act cyclic pentapeptide ring conformations in the complex are similar to those for free Act in the crystal except for a change in orientation of the ester linkage connecting meVal and Thr residues. The cyclic pentapeptide rings are positioned in the minor groove with the established G-C sequence specificity of binding associated with intermolecular hydrogen bonds between the Thr backbone CO and NH groups to the NH_2-2 and N3 positions of guanosine, respectively. Complex formation is also stabilized by van der Waals interactions between nonpolar groups on the cyclic pentapeptide rings and the sugar residues and base pair edges lining the widened minor groove of the $(A3\text{-}G4\text{-}C5\text{-}T6)_I{\cdot}(A3\text{-}G4\text{-}C5\text{-}T6)_{II}$ binding site segment of the DNA helix.

* To whom correspondence should be addressed.

INTRODUCTION

The antitumor drug actinomycin D **1** (designated Act) binds to DNA (reviewed in Reich and Goldberg, 1964; Waring, 1981) through intercalation of the planar phenoxazone ring into the double helix (Muller and Crothers, 1968; Waring, 1970) and inhibits transcription. The early binding studies of Act to DNA established a requirement for the 2-amino group of purines and the presence of a purine (3′-5′) pyrimidine step (Cerami et al., 1967; Wells and Larson, 1970). Chemical (Van Dyke et al., 1982) and enzymatic (Fox and Waring, 1984) footprinting studies demonstrated that the Act binding site was centered around one or more G·C base pairs in duplex DNA. Optical titration studies established that Act intercalates preferentially at G-C steps at the deoxydinucleotide (Krugh, 1972) and deoxyoligonucleotide (Patel and Canuel, 1977) level.

X-ray structures are available for free Act (Ginell et al., 1988) and its complexes with two equivalents of dG (Sobell et al., 1971; Jain and Sobell, 1972) and two equivalents of d(G-C) (Takusagawa et al., 1982). The structure of Act is similar in all these crystals with the cyclic pentapeptide lactone rings aligned on either side of the phenoxazone chromophore and related by a pseudo twofold axis of symmetry. A model has been proposed for intercalation of Act at G-C steps in a DNA oligomer duplex (Sobell and Jain, 1972; Sobell, 1973) but attempts to verify the intercalation complex crystallographically remain unsuccessful to date. The model suggests Act intercalation through the minor groove with its cyclic pentapeptide lactone rings spanning two base pairs on either side of the intercalation site. Sequence specificity for G-C steps is associated with intermolecular hydrogen bonds involving the 2-amino group of deoxyguanosines and the carbonyl oxygen of L-threonine on the cyclic pentapeptide lactone rings.

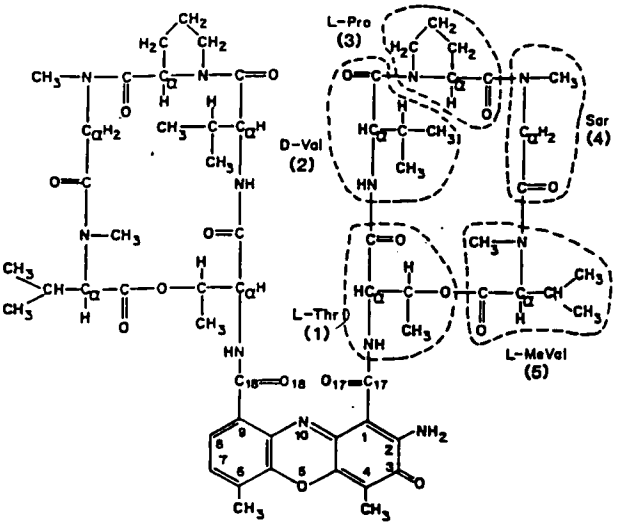

Actinomycin D

1

High-resolution proton NMR spectroscopy has been applied extensively to characterize structural features of Act–DNA oligomer complexes. These studies have been undertaken on DNA oligomer sequences containing single G-C steps and include complexes with d(G-C) (Krugh and Neely, 1973; Patel, 1974a,1976a; Krugh and Chen, 1975; Brown et al., 1982), d(C-G-C-G) (Patel, 1976b; Petersheim et al., 1984; Delepierre et al., 1989), d(A-G-C-T) (Reid et al., 1983; Delepierre et al., 1989) and d(A-T-G-C-A-T) (Patel, 1974b; Brown et al., 1984; Creighton et al., 1989). NMR studies have also been reported on the binding of Act and netropsin at adjacent G·C and A·T rich regions, respectively, on duplex DNA (Patel et al., 1981). The proton and phosphorus NMR parameters demonstrate that the twofold symmetry of these self-complementary DNA oligomer sequences is broken on Act complex formation. The NMR data establish intercalation of the phenoxazone ring between G·C base pairs such that the quinonoid edge is directed towards one strand and the benzenoid edge is directed towards the other strand in the complex. The pentapeptide lactone rings are positioned in the minor groove and make hydrophobic interactions consistent with the general features of the Sobell (1973) model for the complex.

We have characterized the complex of one equivalent of Act with the d(A-A-A-G-C-T-T-T) self-complementary duplex which serves as the control complex containing a single G-C binding site. The combined use of NMR and molecular dynamics to characterize the Act–DNA oligomer complexes uses methodology previously applied in our laboratory to characterize DNA oligomer complexes with the G·C specific minor groove binding agent chromomycin (Gao and Patel, 1989; Gao et al., 1991), the intercalator nogalamycin (Zhang and Patel, 1990) and the bisintercalators echinomycin (Gao and Patel, 1988) and luzopeptin (Zhang and Patel, 1991).

This structural study of the Act-d(A_3GCT_3) complex (1 drug per duplex) and a companion structural study of the Act–d(A_2GCGCT_2) complex (2 drugs per duplex) (Liu and Patel, in preparation) provide new insights into the binding of Act at isolated G-C and adjacent G-C-G-C sites on duplex DNA.

MATERIALS AND METHODS

Oligonucleotide synthesis

The self-complementary d(A_3GCT_3) duplex was synthesized on a 10-μmol scale on a Pharmacia Gene Assembler Plus Synthesizer using the solid-phase cyanoethyl phosphoramidite method. The general procedures for synthesis, deprotection and purification have been reported elsewhere (Zhang and Patel, 1990).

Actinomycin–DNA oligomer complex

Actinomycin-D was purchased from Sigma and used without further purification. The complex was prepared by adding aliquots of solid Act to the DNA oligomer duplex and monitoring complex formation by proton NMR. The free duplex and complex were in slow exchange and the titration could be readily followed by monitoring peak intensities. The addition was stopped on formation of the Act–d(A_3GCT_3) complex (1 drug per duplex). Free Act is insoluble at ambient temperature and can be readily separated by centrifugation.

NMR experiments

NMR spectra were recorded on Bruker AM 400 and AM 500 spectrometers at Columbia

University and on the AM 600 spectrometer at the National NMR Center at the University of Wisconsin.

NOESY spectra on the complexes in H_2O solution were recorded at a mixing time of 200 ms. The corresponding NOESY spectra on the complexes in D_2O were recorded at mixing times of 30, 60, 90, 120, 150 and 200 ms. HOHAHA spectra were recorded at spin-lock times of 55, 80 and 97 ms on the complexes in D_2O solution. The acquisition and processing parameters are similar to those reported previously (Zhang and Patel, 1990). All two-dimensional NMR data sets were processed using FTNMR (Hare Research) on either a VAX 11-780 or a microVAX II running VMS and were plotted on either ZETA 822 or HP 7475A plotters.

Interproton distance constraints

The buildup of the volume integrals of the assigned NOESY cross peaks were measured in NOESY spectra recorded as a function of mixing time between 30 ms and 200 ms. The initial slopes were computed and approximate distances estimated using the two-spin approximation and calibration against buildups for fixed interproton distances. The interproton distances involving base-base, base-sugar H1′ and phenoxazone-base protons were calculated using the cytidine H6-H5 distance of 2.5 Å as a reference, those involving methyl groups were calculated using the thymidine H6-CH_3 distance of 2.9 Å as a reference and those involving all other nonexchangeable protons were calculated using the sugar H2′-H2″ distance of 1.8 Å as a reference. Each distance was bracketed by a lower and upper bound which was set to $\pm$ 15% for the nonexchangeable protons and $\pm$ 1.0 Å for the exchangeable protons in the complex.

Molecular dynamics calculations

The initial models of the Act–d(A_3GCT_3) (1 drug per duplex) complex were generated using either MACROMODEL (W.C. Still, Columbia University) or QUANTA (Polygen Corporation). All energy minimization and molecular dynamics calculations were carried out on a Convex C2 computer using the XPLOR program (A. Brunger, Yale University). The general procedure for the energy minimization and molecular dynamics calculations have been described previously (Zhang and Patel, 1990). Two different starting models were generated for the complex and the refinement guided by the input distance constraints available from the NMR analysis.

Each of the initial structures was first subjected to 300 cycles of energy minimization in order to relieve bad contacts between nonbonded atoms. During this energy minimization, the hydrogen-bond constraints for DNA base pairs were used to retain Watson-Crick pairing in the DNA oligomer duplex. The structure was then subjected to molecular dynamics refinements in two stages, namely, a high-temperature stage and a cooling/equilibration stage. In the high-temperature stage, integration of Newton's equations of motion was performed by a Verlet integration algorithm with initial velocities assigned to a Maxwell distribution at 300 K. A loop with 10 cycles was used to gradually introduce the NOE restraints by increasing the NOE scale factor. The time step was set to be 0.0004 ps, and 250 steps dynamics were run for each NOE scale factor. The system was heated up without rescaling the velocities of the atoms at the end of each 250-step dynamics calculation, unless the temperature of the system exceeded 2000 K. In the cooling/equilibration stage, the NOE scale factor was set to 0.2 and 5 for the two final Act–d(A_3GCT_3) complex structures. Integration of Newton's equations of motion was also performed by a Verlet integration algorithm with initial velocities assigned to a Maxwell distribution at 300 K. The temperature of the

system was maintained at 300 K by rescaling the velocities of the atoms every 0.250 ps. The time step of the integrator was 0.001 ps. The structure was then further refined by restrained energy minimization.

RESULTS

Complex formation and stoichiometry

We have generated the Act–d(A_3GCT_3) complex (1 drug per duplex) by monitoring the imino protons of the duplex on gradual addition of Act in H_2O solution at low temperature. The free duplex and the complex are in slow exchange. The twofold symmetry of the self-complementary d(A_3GCT_3) duplex is lifted on Act complex formation so that separate resonances are detected at

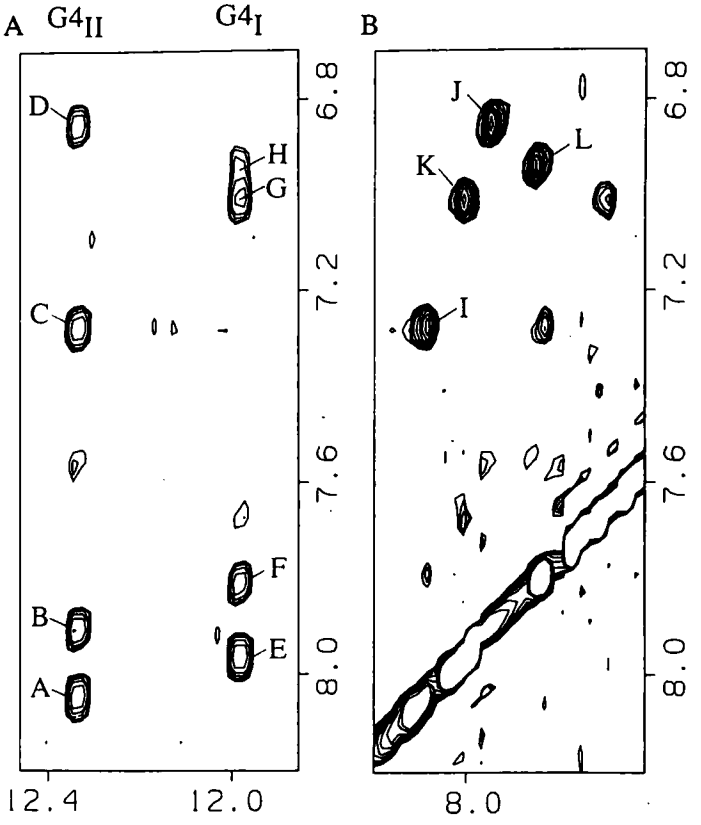

Fig. 1. Expanded NOESY contour plots (mixing time 200 ms) for the Act–d(A_3GCT_3) complex in H_2O buffer, pH 6.5 at 15°C, correlating (A) distance connectivities between guanosine imino protons (11.9–12.5 ppm) and amino protons (6.7–8.2 ppm) and (B) distance connectivities between 7.6–8.3 ppm and 6.7–8.2 ppm amino proton regions. The cross peaks A–H are assigned as follows. A: $G4_{II}$(NH1)-$G4_{II}$(NH_2-2b); B: $G4_{II}$(NH1)-$C5_I$(NH_2-4b); C: $G4_{II}$(NH1)-$G4_{II}$(NH_2-2e); D: $G4_{II}$(NH1)-$C5_I$(NH_2-4e); E: $G4_I$(NH1)-$G4_I$(NH_2-2b); F: $G4_I$(NH1)-$C5_{II}$(NH_2-4b); G: $G4_I$(NH1)-$G4_I$(NH_2-2e); H: $G4_I$(NH1)-$C5_{II}$(NH_2-4e). The cross peaks I–L are assigned as follows: I: $G4_{II}$(NH_2-2b)-$G4_{II}$(NH_2-2e); J: $C5_I$(NH_2-4b)-$C5_I$(NH_2-4e); K: $G4_I$(NH_2-2b)-$G4_I$(NH_2-2e); L: $C5_{II}$(NH_2-4b)-$C5_{II}$(NH_2-4e). The symbols b and e for NH_2 protons designate hydrogen bonded and exposed, respectively.

11.97 and 12.33 ppm for the imino protons of the G4·C5 base pairs in the complex. By contrast, a single broad resonance at 13.94 ppm is observed for the T6 imino proton of the A3·T6 base pair in the complex. This result establishes that the non-equivalence of the two strands in the Act–d(A_3GCT_3) complex will be pronounced at the G4-C5 binding site but taper off on proceeding towards the end of the helix. We designate the two strands I and II in the complex with the benzenoid edge of the intercalated phenoxazone directed towards strand II and the quinonoid edge directed towards strand I (see below).

Exchangeable nucleic acid protons in complex

We have recorded the NOESY spectrum (200 ms mixing time) of the Act–d(A_3GCT_3) complex in H_2O buffer, pH 6.5 at 15°C. An expanded contour plot establishing distance connectivities between the guanosine imino protons (11.9–12.5 ppm) and amino protons (6.7–8.2 ppm) is plotted in Fig. 1A. We note that the imino protons of $G4_I$ (strand I) and $G4_{II}$ (strand II) each exhibit four NOE cross peaks in the amino proton region. These peaks must represent NOEs to the hydrogen-bonded and exposed amino protons of guanosine and cytidine within the G·C base pair (Fig. 1B). These amino protons can be distinguished since the cytidine amino protons exhibit

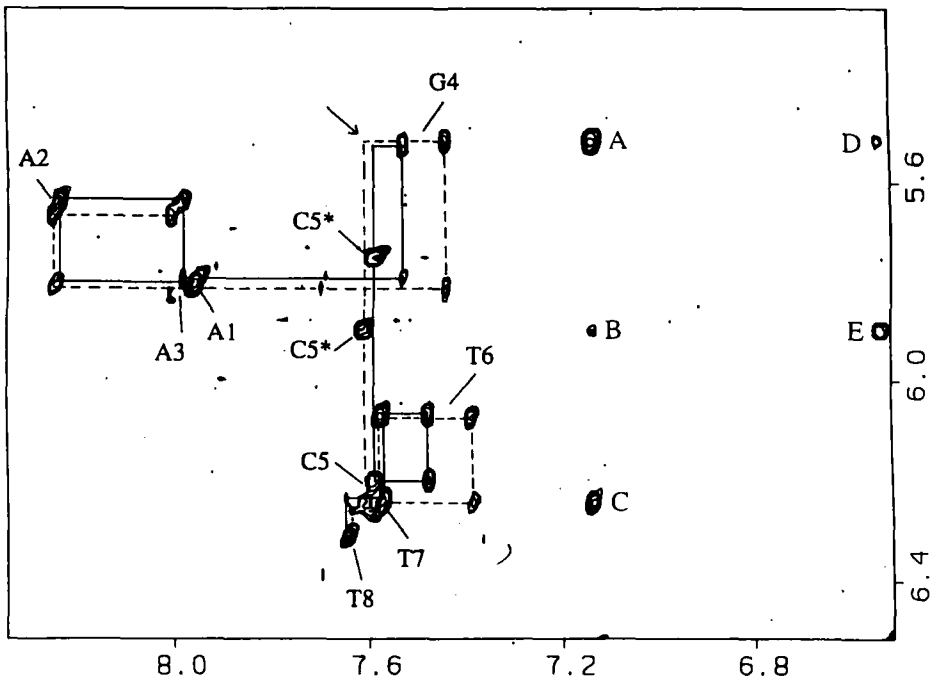

Fig. 2. Expanded NOESY contour plots (mixing time 250 ms) for the Act–d(A_3GCT_3) complex in D_2O buffer, pH 6.5 at 15°C, correlating distance connectivities between base protons (6.5–8.3 ppm) and the sugar H1′ and cytidine H5 protons (5.2–6.5 ppm). The tracing outlines connectivities between base protons and their own and 5′-flanking sugar H1′ protons. The solid tracing is for strand I and the dashed tracing is for strand II in the complex. The assignments correspond to NOEs between base protons and their own sugar H1′ protons. The NOEs between cytidine H6 and H5 protons are designated by asterisks. The cross peaks A–E are assigned as follows: A: Act(H8)-$G4_{II}$(H1′); B: Act(H8)-$C5_{II}$(H5); C: Act(H8)-$C5_{II}$(H1′); D: Act(H7)-$G4_{II}$(H1′); E: Act(H7)-$C5_{II}$(H5).

NOEs to the cytidine H5 proton while the guanosine amino protons exhibit weak NOEs to the guanosine H1′ protons. Thus, the $G4_{II}$ imino proton exhibits NOEs to the hydrogen-bonded and exposed amino protons of $G4_{II}$ (peaks A and C, respectively, Fig. 1A) and the hydrogen-bonded and exposed amino protons of $C5_I$ (peaks B and D, respectively, Fig. 1A).

The 2-amino protons of guanosine are located in the minor groove while the 4-amino protons of cytidine are located in the major groove so that both minor and major groove markers are available at the non-equivalent $G4_I$·$C5_{II}$ and $G4_{II}$·$C5_I$ base pairs in the Act–d(A_3GCT_3) complex. The observation of separate hydrogen-bonded and exposed amino protons of G4 establishes slow rotation around the C-NH_2 bond in the complex.

Nonexchangeable nucleic acid protons in complex

The nonexchangeable proton spectrum (0.5–8.5 ppm) of the Act–d(A_3GCT_3) complex in D_2O buffer exhibits sufficiently narrow and partially resolved resonances for further characterization by two-dimensional NMR techniques. We have recorded NOESY spectra (mixing times ranging from 30 ms to 250 ms) on the Act–d(A_3GCT_3) complex in D_2O buffer, pH 6.5 at 15°C. An expanded plot (mixing time 250 ms) establishing distance connectivities between the base protons (6.5–8.3 ppm) and the sugar H1′ and cytidine H5 protons (5.2–6.5 ppm) is shown in Fig. 2. For regular right-handed DNA duplexes, the base proton (purine H8 or pyrimidine H6) exhibits NOEs to its own and 5′-flanking sugar H1′ protons permitting an NOE walk from the 5′ to the 3′

TABLE I
NUCLEIC ACID PROTON CHEMICAL SHIFTS IN THE Act–d(A_3GCT_3) COMPLEX (1 DRUG PER DUPLEX)

Residue	Chemical shifts (ppm)								
	NH	NH_2	H8	H2	H6	H5/CH_3	H1′	H2′, 2″	H3′	H4′
Strand I										
A1			7.95				5.81	2.26, 2.41	4.79	4.12
A2			8.24				5.65	2.78	5.02	4.35
A3			7.98	7.68			5.80	2.36	5.00	4.25
G4	11.97	7.01, 7.96	7.53				5.53	2.42, 2.67	5.00	3.80
C5		6.85, 7.91			7.59	5.76	6.20	2.33, 2.36	4.65	3.71
T6	13.94				7.48	1.77	6.08	2.16, 2.56	4.85	3.97
T7					7.57	1.87	6.24	2.42, 2.58	4.87	4.22
T8					7.64	1.83	6.31	2.33	4.62	4.13
Strand II										
A1			7.96				5.81	2.29, 2.45	4.81	4.12
A2			8.25				5.67	2.84	5.02	4.37
A3			8.01	7.55			5.83	2.42, 2.48	5.00	4.33
G4	12.33	7.27, 8.05	7.44				5.52	2.49, 2.66	5.03	3.82
C5		6.94, 7.81			7.61	5.90	6.24	1.95, 2.57	4.52	3.85
T6	13.94				7.38	1.78	6.07	2.12, 2.59	4.86	3.94
T7					7.58		6.26	2.43, 2.62	4.94	4.20
T8					7.64		6.31	2.33	4.61	4.13

terminus of each strand in the duplex (see review by van de Ven and Hilbers, 1988). The non-equivalence of the two strands results in separate tracings in the complex as shown in Fig. 2. The tracing of the strand designated II is shown by dashed lines while the tracing of the strand designated I is shown by full lines. We detect NOEs between the H8 proton on the benzenoid edge of the phenoxazone ring and the minor groove sugar H1′ protons of G4 (peak A, Fig. 2) and C5 (peak C, Fig. 2) of strand II in the complex. This defines strand II as the one directed towards the benzenoid edge of the phenoxazone ring of Act in the complex. These data provide the base and sugar H1′ proton assignments for strands I and II in the Act–d(A_3GCT_3) complex. A similar analysis has been undertaken on the nucleic acid protons in the remainder of the NOESY spectrum to assign the sugar H2′, H2″, H3′ and H4′ protons on both strands in the complex (Table 1). The nonexchangeable proton chemical shifts for a particular proton show small differences between strands I and II with the largest shift difference being observed for the base H5 and sugar H2′ and H2″ protons of C5 in the complex (Table 1). This results in increased spectral overlap of intra-

TABLE 2
ACTINOMYCIN PROTON CHEMICAL SHIFTS IN Act–d(A_3GCT_3) COMPLEX (1 DRUG PER DUPLEX)

Residue	Chemical shifts (ppm)			
	Position	Aromatic	Quinonoid (Q)	Benzenoid (B)
Phenoxazone	H8	7.13		
	H7	6.54		
	6-CH_3	1.85		
	4-CH_3	1.76		
L-Thr	α		4.57	4.79
	β		5.24	5.24
	γ		1.39	1.41
	NH		7.69	7.85
D-Val	α		3.67	3.67
	β		2.16	2.16
	γ		1.08, 0.86	1.08, 0.86
	NH		8.10	8.12
L-Pro	α		6.39	6.37
	β		3.34, 2.00	3.25, 2.16
	γ		3.99, 2.10	3.91, 2.29
	δ		2.10	2.08
Sar	α		4.50, 4.34	4.59, 4.39
	NCH_3		2.99	3.03
L-meVal	α		2.89	2.85
	β		2.56	2.53
	γ		0.94, 0.91	0.94, 0.91
	NCH_3		2.89	2.98

molecular and intermolecular NOEs involving protons related by pseudo-symmetry as one proceeds in either direction from the center towards either end of the Act–d(A_3GCT_3) complex.

There must be a disruption in the helical parameters at the G4-C5 steps on both strands in the Act–d(A_3GCT_3) complex since the NOEs between the H6 of C5 and the H1′ of G4 are absent in the dashed line tracing for strand II and the full line tracing for strand I (see arrow in Fig. 2). Such a disruption would result from intercalation of the phenoxazone ring of Act between G·C pairs at the G4-C5 step in the d(A_3GCT_3) duplex on complex formation.

Nonexchangeable Act protons in complex

Act **1** lacks an exact twofold element of symmetry since its phenoxazone chromophore contains a benzenoid and a quinonoid edge. The cyclic pentapeptide lactone rings which project in either

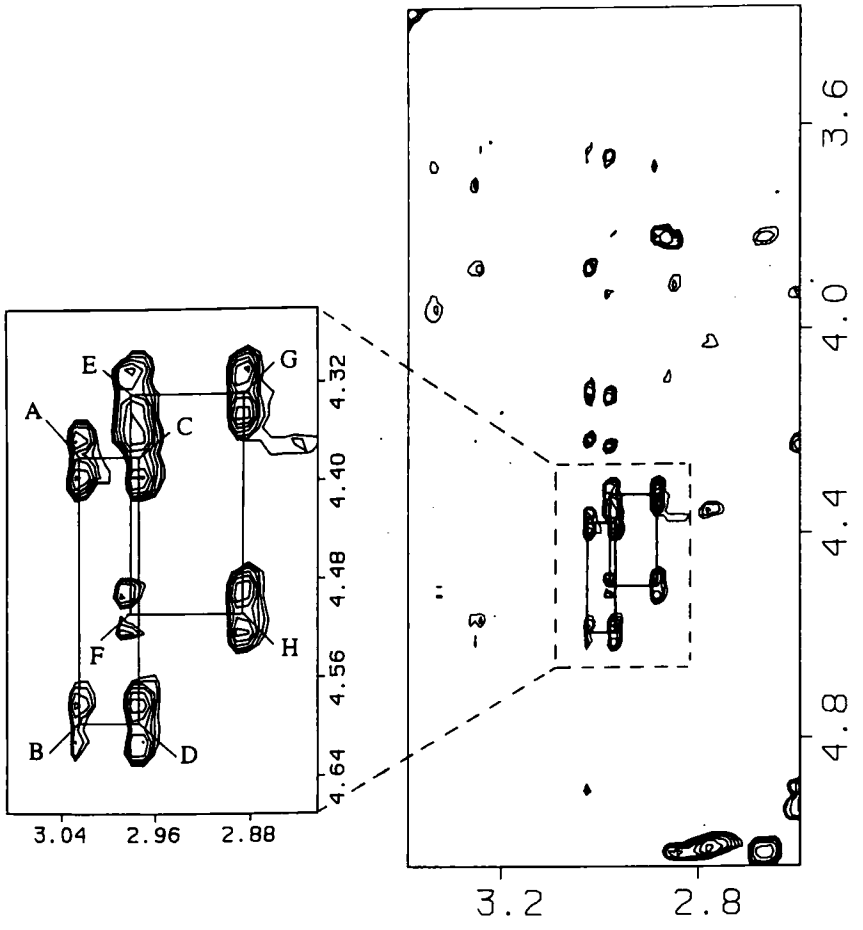

Fig. 3. Expanded NOESY contour plots (mixing time 250 ms) for the Act–d(A_3GCT_3) complex in D_2O buffer, pH 6.5 at 15°C, correlating distance connectivities between 2.6–3.4 ppm and 3.4–4.0 ppm regions. The cross peaks A–H are assigned as follows. A: $Sar_B(NCH_3)$-$Sar_B(H^{\alpha}B)$; B: $Sar_B(NCH_3)$-$Sar_B(H^{\alpha}A)$; C: $meVal_B(NCH_3)$-$Sar_B(H^{\alpha}B)$; D: $meVal_B(NCH_3)$-$Sar_B(H^{\alpha}A)$; E: $Sar_Q(NCH_3)$-$Sar_Q(H^{\alpha}B)$; F: $Sar_Q(NCH_3)$-$Sar_Q(H^{\alpha}A)$; G: $meVal_Q(NCH_3)$-$Sar_Q(H^{\alpha}B)$; H: $meVal_Q(NCH_3)$-$Sar_Q(H^{\alpha}A)$.

direction from the phenoxazone ring are designated B for the one that is covalently linked to the benzenoid ring and Q for the one that is covalently linked to the quinonoid ring. The cyclic pentapeptide rings contain the sequence (L-Thr)-(D-Val)-(L-Pro)-(Sar)-(L-meVal). It has been possible using standard through-space distance (in NOESY spectra) and through-bond coupling (in COSY and HOHAHA spectra) connectivities (Wüthrich, 1986) to completely assign the peptide protons within each of the cyclic pentapeptide rings in the Act–d(A_3GCT_3) complex (Table 2). The expanded NOESY contour plot (mixing time 250 ms) in Fig. 3 focuses on NOE connectivities

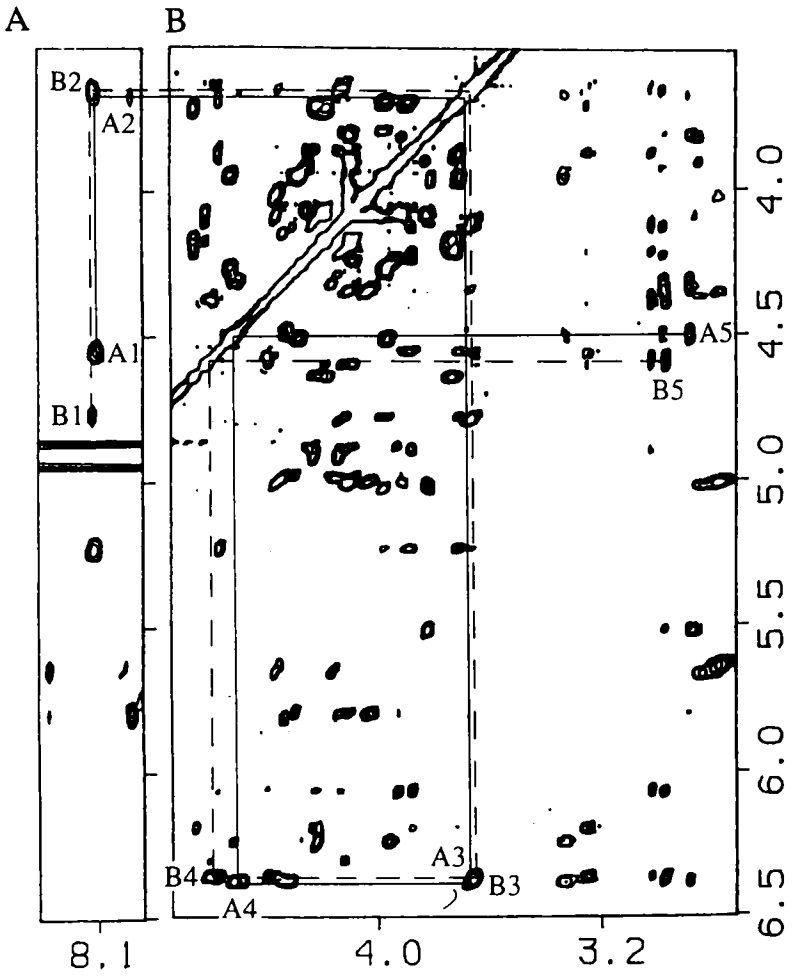

Fig. 4. (A) Expanded NOESY contour plots (mixing time 200 ms) for the Act–d(A_3GCT_3) complex in H_2O buffer, pH 6.5 at 10°C, correlating distance connectivities between the 7.9–8.3 ppm and the 3.5–6.5 ppm regions. (B) Expanded NOESY contour plots (mixing time 250 ms) for the Act–d(A_3GCT_3) complex in D_2O buffer, pH 6.5 at 15°C, correlating distance connectivities between the 2.6–4.8 ppm and the 3.5–6.5 ppm regions. The cross peaks A1–A5 follow connectivities in the quinonoid cyclic pentapeptide ring and are assigned as follows: A1: $Thr_Q(H^\alpha)$-$Val_Q(NH)$; A2: $Val_Q(NH)$-$Val_Q(H^\alpha)$; A3: $Val_Q(H^\alpha)$-$Pro_Q(H^\alpha)$; A4: $Pro_Q(H^\alpha)$-$Sar_Q(H^\alpha B)$; A5: $Sar_Q(H^\alpha B)$-$meVal_Q(NCH_3)$. The cross peaks B1–B5 follow connectivities in the benzenoid cyclic pentapeptide ring and are assigned as follows: B1: $Thr_B(H^\alpha)$-$Val_B(NH)$; the intensity of this strong cross peak is attenuated by its proximity to the H_2O resonance; B2: $Val_B(NH)$-$Val_B(H^\alpha)$; B3: $Val_B(H^\alpha)$-$Pro_B(H^\alpha)$; B4: $Pro_B(H^\alpha)$-$Sar_B(H^\alpha B)$; B5: $Sar_B(H^\alpha B)$-$meVal_B(NCH_3)$.

between the geminal Sar H^{α} protons (designated HαA and HαB) at 4.2 and 4.7 ppm and the NCH_3 protons of Sar and meVal at 2.8 and 3.1 ppm. As an example, the NOE between the meVal(NCH_3) proton and the Sar(HαB) proton on the benzenoid cyclic pentapeptide ring (peak D, Fig. 3) is distinct from that on the quinonoid cyclic pentapeptide ring (peak H, Fig. 3) in the complex. The corresponding connectivities for the benzenoid (peaks A–D, Fig. 3) and quinonoid (peaks E–H, Fig. 3) rings (cross-peak assignments are listed in caption to Fig. 3) establish small but distinct differences in the chemical shifts of the same protons in the two cyclic pentapeptide rings in the Act–d(A_3GCT_3) complex. A comparison of proton chemical shifts (Table 2) establishes that the largest difference between the two cyclic pentapeptide rings is detected for the NH and Hα protons of L-Thr in the complex. This is not surprising since these protons are separated by the fewest bonds from the phenoxazone ring and should monitor the different ring current contributions from the benzenoid and quinonoid ring systems.

Peptide and ester linkages of Act in complex

The crystal structure of free Act exhibits *trans* peptide linkages between Thr-Val and Sar-meVal steps and *cis* peptide linkages between Val-Pro and Pro-Sar steps around the cyclic pentapeptide rings (Ginell et al., 1988). The nature of the peptide linkages in the Act–d(A_3GCT_3) complex can be determined from the relative magnitude of the NOEs between NH and Hα protons on adjacent residues, between H^{α} protons on adjacent residues and between H^{α} and NCH_3 protons on adjacent residues. This is demonstrated for the peptide and ester linkages in the quinonoid cyclic pentapeptide ring in the complex as shown below. We detect a strong NOE between the H^{α} of Thr_Q and the NH of Val_Q (peak A1, Fig. 4A) establishing a *trans* Thr_Q-Val_Q peptide linkage. The strong NOE cross peaks between the Hα protons of Val_Q and Pro_Q (peak A3, Fig. 4B) and between the Hα protons of Pro_Q and Sar_Q (peak A4, Fig. 4B) establish *cis* peptide linkages at both Val_Q-Pro_Q and Pro_Q-Sar_Q steps. Finally, a strong NOE is detected between the Hα proton of Sar_Q and the NCH_3 protons of $meVal_Q$ establishing a *trans* peptide linkage at the Sar-meVal step in the complex (peak A5, Fig. 4B). The corresponding trace for the benzenoid cyclic pentapeptide ring (cross peaks B1 and B3 to B5, Fig. 4) are consistent with the Thr-Val and Sar-meVal linkages being *trans* and the Val-Pro and Pro-Sar linkages being *cis* also for the benzenoid cyclic pentapeptide ring in the complex.

Intermolecular NOEs in complex

The intermolecular NOEs in the NOESY spectrum of the Act–d(A_3GCT_3) complex have been identified following characterization of the Act and nucleic acid proton chemical shifts. Typical intermolecular NOEs are identified in an expanded NOESY contour plot (250 ms mixing time) of the Act–d(A_3GCT_3) complex (peaks A–W, Fig. 5). An interesting question relates to whether resolved intermolecular NOEs are observed between the same pair of protons in the pseudo-symmetric halves of the complex. In general, the intermolecular NOE cross peaks at the central G4-C5 Act binding site are better resolved between the two halves of the molecule and this resolution is reduced significantly on proceeding towards the ends of the helix in the complex (Fig. 5).

The intermolecular NOEs in the Act–d(A_3GCT_3) complex are listed in Table 3 and classified as to their origin in the phenoxazone, benzenoid and quinonoid cyclic pentapeptide rings of the drug. The following general conclusions can be reached from the listed intermolecular NOEs in the complex. The phenoxazone ring of Act intercalates at the G4-C5 step in the d(A_3GCT_3)

duplex such that the edge containing the CH_3-4 and CH_3-6 groups projects into the major groove. The former conclusion is based on NOEs from the CH_3 protons to the imino protons of $G4_I$ and $G4_{II}$ while the latter conclusion is based on NOEs from the CH_3 protons to the major groove amino protons of $C5_I$ and $C5_{II}$. The benzenoid edge is directed towards the $G4_{II}$-$C5_{II}$ sugar-phosphate backbone based on NOEs between the H7 and H8 protons and the base and sugar protons of these two residues in the complex (Table 3).

The cyclic pentapeptide rings are positioned in the minor groove based on the extensive NOEs observed between their protons and the sugar H1′ and H4′ nucleic acid protons in the complex (Table 3). Each cyclic pentapeptide ring forms intermolecular contacts with both strands of the duplex in the complex. Thus, for the quinonoid cyclic pentapeptide ring, Pro_Q is positioned opposite $C5_{II}$, $meVal_Q$ is positioned opposite $G4_I$ and Sar_Q is positioned opposite the $A3_I$·$T6_{II}$ base pair in the complex (Table 3). These results establish the intermolecular alignments of the amino acid

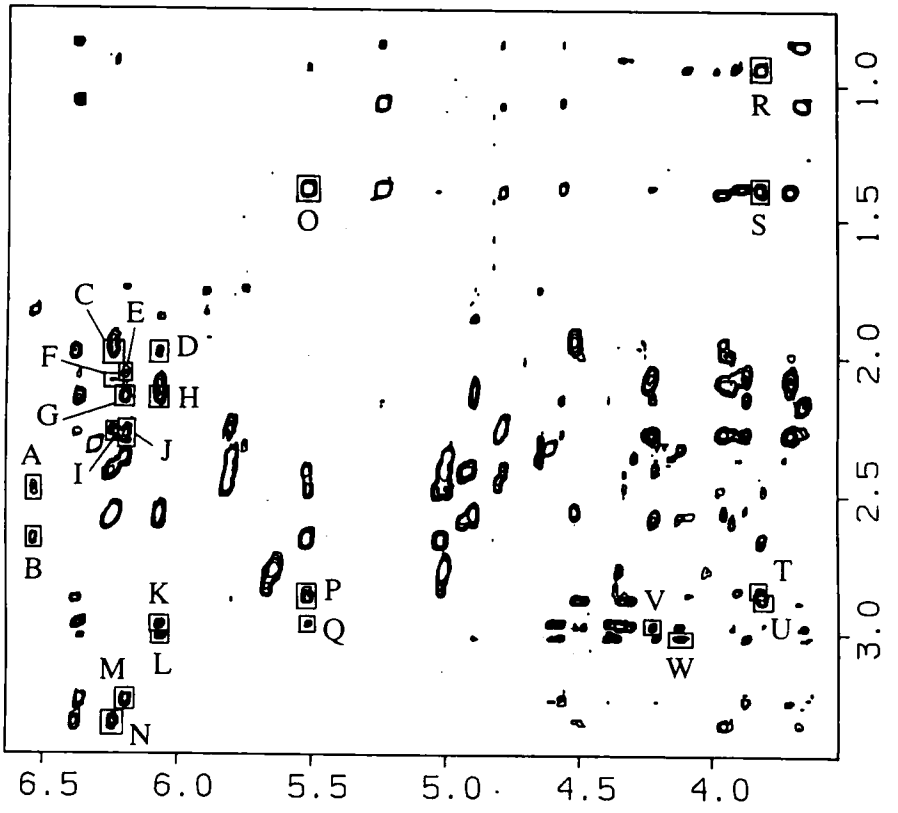

Fig. 5. An expanded NOESY contour plot (mixing time 250 ms) for the Act–d(A_3GCT_3) complex in D_2O buffer, pH 6.5 at 15°C, correlating distance connectivities between the 3.5–6.7 ppm and 0.8–3.4 ppm regions. The cross peaks A–W are assigned as follows: A: Act(H7)-$G4_{II}$(H2′); B: Act(H7)-$G4_{II}$(H2″); C: $Pro_Q(H^{\beta}B)$-$C5_{II}$(H1′); D: $Pro_Q(H^{\beta}B)$-$T6_{II}$(H1′); E: $Pro_B(H^{\gamma}A)$-$C5_I$(H1′); F: $Pro_Q(H^{\gamma}A)$-$C5_{II}$(H1′); G: $Pro_B(H^{\beta}B)$-$C5_I$(H1′); H: $Pro_B(H^{\beta}B)$-$T6_I$(H1′); I: $Pro_Q(H^{\gamma}B)$-$C5_{II}$(H1′); J: $Pro_B(H^{\gamma}B)$-$C5_I$(H1′); K: $Sar_Q(NCH_3)$-$T6_{II}$(H1′); L: $Sar_B(NCH_3)$-$T6_I$(H1′); M: $Pro_B(H^{\beta}A)$-$C5_I$(H1′); N: $Pro_Q(H^{\beta}A)$-$C5_{II}$(H1′); O: $Thr_{B,Q}(CH_3{}^{\gamma})$-$G4_{I,II}$(H1′); P: $meVal_{B,Q}(H^{\alpha})$-$G4_{I,II}$(H1′); Q: $meVal_B(NCH_3)$-$G4_{II}$(H1′); R: $meVal_{B,Q}(CH^{\gamma})$-$G4_{I,II}$(H4′); S: $Thr_{B,Q}(CH_3{}^{\gamma})$-$G4_{I,II}$(H4′); T: $meVal_B(H^{\alpha})$-$G4_{II}$(H4′); U: $meVal_Q(H^{\alpha})$-$G4_I$(H4′); V: $Sar_Q(NCH_3)$-$T7_{II}$(H4′); W: $Sar_B(NCH_3)$-$T7_I$(H4′).

TABLE 3
INTERMOLECULAR NOEs BETWEEN Act AND DNA OLIGOMER PROTONS IN Act–d(A_3GCT_3) COMPLEX (1 DRUG PER DUPLEX)[a]

Phenoxazone protons	*DNA protons*
Act(CH_3-4)	$G4_{II}$(NH3), $C5_I$(NH_2-4b,e)
Act(CH_3-6)	$G4_I$(NH3), $C5_{II}$(NH_2-4b,e)
Act(H8)	$G4_{II}$(H8,H1′, H2′, H2″, H3′), $C5_{II}$(H1′, H4′)
Act(H7)	$G4_{II}$(H8, H2′, H2″), $C5_{II}$(H5, H6)
Quinonoid pentapetide protons	*DNA protons*
Thr_Q(CH_3^γ)	$G4_I$(H1′, H2″, H4′)
Thr_Q(NH)	$G4_I$(NH_2-2e, H1′)
Pro_Q($H^\beta A$)	$C5_{II}$(H1′, H4′), $T6_{II}$(H1′)
Pro_Q($H^\beta B$)	$C5_{II}$(H1′), $T6_{II}$(H1′)
Pro_Q($H^\gamma A$, $H^\gamma B$)	$C5_{II}$(H1′)
Pro_Q($H^\delta B$)	$C5_{II}$(H2′, H4′)
Sar_Q($H^\alpha A$, $H^\alpha B$)	$A3_I$(H2), $T6_{II}$(H1′)
Sar_Q(NCH_3)	$T6_{II}$(H1′), $T7_{II}$(H4′)
$meVal_Q$(H^α)	$G4_I$(H1′, H4′)
$meVal_Q$(CH_3^γ)	$G4_I$(H4′)
$meVal_Q$(NCH_3)	$A3_I$(H2), $G4_I$(H1′, NH3, NH_2-2b,e)
Benzenoid pentapeptide protons	*DNA protons*
Thr_B(CH_3^γ)	$G4_{II}$(H1′, H2″, H4′)
Thr_B(NH)	$G4_{II}$(NH_2-2e, H1′)
Pro_B(H^α)	$T6_I$(H1′)
Pro_B($H^\beta A$, $H^\beta B$)	$C5_I$(H1′), $T6_I$(H1′)
Pro_B($H^\gamma A$)	$C5_I$(H1′)
Pro_B($H^\gamma B$)	$C5_I$(H1′; H5′)
Pro_B($H^\delta B$)	$C5_I$(H2′)
Sar_B($H^\alpha A$, $H^\alpha B$)	$A3_{II}$(H2), $T6_I$(H1′)
Sar_B(NCH_3)	$T6_I$(H1′), $T7_I$(H4′)
$meVal_B$(H^α)	$G4_{II}$(H1′, H4′)
$meVal_B$(CH_3^γ)	$G4_{II}$(H4′)
$meVal_B$(NCH_3)	$A3_{II}$(H2), $G4_{II}$(H1′, NH3, NH_2-2b,e)

[a] NOESY data set (mixing time 200 ms) in H_2O buffer, pH 6.5 at 15°C. NOESY data set (buildup curves based on mixing times of 30, 60, 90, 120 and 150 ms) in D_2O buffer, pH 6.5 at 15°C.

components of the cyclic pentapeptide in relation to the minor groove base pair edges and the sugar residues in the nucleic acid in the complex. Each pentapeptide lactone ring spans two base pairs (G4·C5 and A3·T6) centered about the phenoxazone intercalation site at the $(G4\text{-}C5)_I$·$(G4\text{-}C5)_{II}$ step.

Experimental distance bounds

We have outlined in the Materials and Methods section the approach used to define lower and upper bounds for proton pairs with a detectable NOE between them in the NOESY spectra of the Act–d(A_3GCT_3) complex at short mixing times. A set of 70 intermolecular distance constraints (Table 4) along with 132 distance constraints between nucleic acid protons and 86 distance con-

straints between actinomycin protons in the complex were incorporated in the molecular dynamics simulation and correspond to a total of 288 constraints for the Act–d(A_3GCT_3) complex.

Starting models for structure refinement

The d(A_3GCT_3) duplex was generated from the coordinates of a standard B-form structure. The previously published coordinates of actinomycin from a crystallographic analysis (Ginell et al., 1988) were used to generate the drug. Two quite different initial structures of the complex were generated for the molecular dynamics computations as a test for the convergence characteristics of the final refined structures. One initial structure of the complex was generated by inserting the phenoxazone ring of actinomycin into the d(A_3GCT_3) duplex at the (G_I-C_I)·(G_{II}-C_{II}) step without increasing the separation between G·C base pairs. The cyclic pentapeptide rings are positioned in the minor groove consistent with the experimental data. Energy minimization of this structure resulted in the formation of an intercalation cavity at the bound phenoxazone site. Structural changes were observed in both the DNA and the drug as a result of the minimization. The bound actinomycin molecule was removed and replaced by another corresponding to that observed in the crystalline state. This initial Act–d(A_3GCT_3) complex is designated Init-A.

TABLE 4
BACKBONE TORSION ANGLES IN THE CYCLIC PENTAPEPTIDE RINGS FOR THE Act–d(A_3GCT_3) COMPLEX IN SOLUTION COMPARED TO VALUES FOR FREE Act IN THE CRYSTAL

Residue	Angle	Atom designation	Act–d(A_3GCT_3)		Act[a]
			Quinonoid	Benzenoid	
L-Thr(1)		C^{α}(1)-C^{β}(1)-O^{β}(1)-C5	112	128	153 ± 12
		C(1)-C^{α}(1)-C^{β}(1)-O^{β}(1)	295	290	304 ± 7
	ψ(Thr)	N(2)-C(1)-C^{α}(1)-C^{β}(1)	289	270	289 ± 5
	ω(Thr)	C^{α}(2)-N(2)-C(1)-C^{α}(1)	180	180	164 ± 6
D-Val(2)	φ(Val)	C(2)-C^{α}(2)-N(2)-C(1)	79	92	76 ± 12
	ψ(Val)	N(3)-C(2)-C^{α}(2)-N(2)	58	62	39 ± 4
	ω(Val)	C^{α}(3)-N(3)-C(2)-C^{α}(2)	20	6	21 ± 10
L-Pro(3)	φ(Pro)	C(3)-C^{α}(3)-N(3)-C(2)	263	284	271 ± 9
	ψ(Pro)	N(4)-C(3)-C^{α}(3)-N(3)	153	145	164 ± 13
	ω(Pro)	C^{α}(4)-N(4)-C(3)-C^{α}(3)	0	0	2 ± 26
Sar(4)	φ(Sar)	C(4)-C^{α}(4)-N(4)-C(3)	270	261	254 ± 18
	ψ(Sar)	N(5)-C(4)-C^{α}(4)-N(4)	171	188	190 ± 9
	ω(Sar)	C^{α}(5)-N(5)-C(4)-C^{α}(4)	180	180	174 ± 6
L-meVal(5)	φ(meVal)	C(5)-C^{α}(5)–N(5)-C(4)	39	22	59 ± 9
	ψ(meVal)	O^{β}(1)-C(5)-C^{α}(5)-N(5)	107	91	50 ± 17
	ω(meVal)	C^{β}(1)-O^{β}(1)-C(5)-C^{α}(5)	198	204	175 ± 5

[a] These values represent an average of the six Act conformations observed in the crystalline state (Ginell et al., 1988).

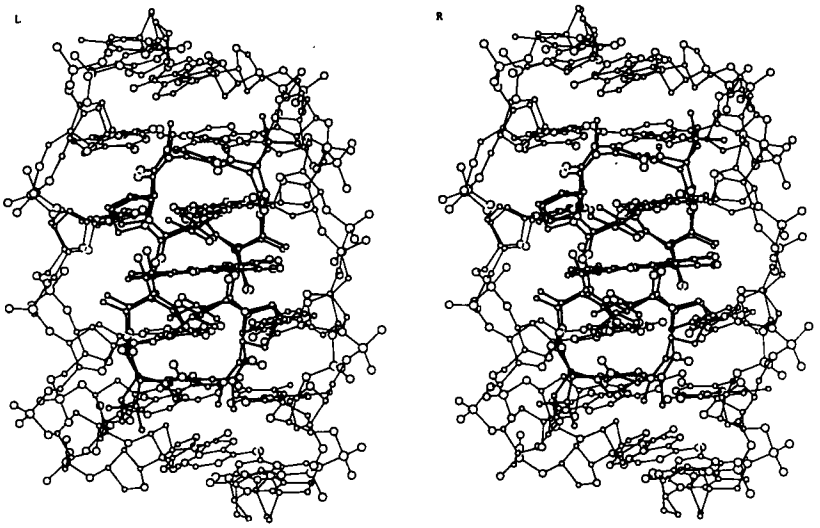

Fig. 6. A stereoview of two superpositioned structures of the Act–d(A_3GCT_3) complex (1 drug per duplex) following molecular dynamics refinement including NMR-based distance constraints. These refined structures were generated from Init-A and Init-B starting structures. The terminal A·T base pairs at either end are deleted.

The second initial structure of the complex was generated by cleaving the d(A_3GCT_3) duplex at G-C steps on both strands and increasing the separation between G·C base pairs by a factor of two. The phenoxazone ring of Act was inserted at the cleavage site with the cyclic pentapeptide rings positioned in the minor groove. This initial structure of the complex, designated Init-B, has the phenoxazone ring inclined relative to the flanking G·C base pairs. Ligation of the backbone atoms on each strand at the intercalation site was achieved during subsequent minimization.

Structure refinement

The initial structures served as starting models for structure refinement using molecular dynamics (MD) computations with NMR-based distance bounds as input constraints. The refinement protocol is outlined in the Materials and Methods Section. The final structures which were refined from two quite different starting structures are superpositioned on the basis of a best fit for all heavy atoms in Fig. 6 and exhibit a root-mean-square deviation of 1.1 Å.

One of these final structures for the Act–d(A_3GCT_3) complex (lacking the terminal A1·T8 base pairs at either end of the helix) is plotted in stereo with emphasis on two different views in Fig. 7. The structure of the Act–d(A_3GCT_3) complex is of the classic intercalative type with the phenoxazone ring sandwiched between G·C pairs and the cyclic pentapeptide rings spanning two base pairs in either direction in the minor groove. The overall topology of the two cyclic pentapeptide rings matches the right-handed orientation of the DNA helix minor groove (Fig. 7A).

Act conformation in the complex

The majority of the conformational parameters of the drug in the Act–d(A_3GCT_3) complex in solution are similar to those of the free drug in the crystal (Tables 4 and 5). Thus, the two cyclic pentapeptide rings are related by a pseudo-twofold axis of symmetry. The *trans* peptide/ester

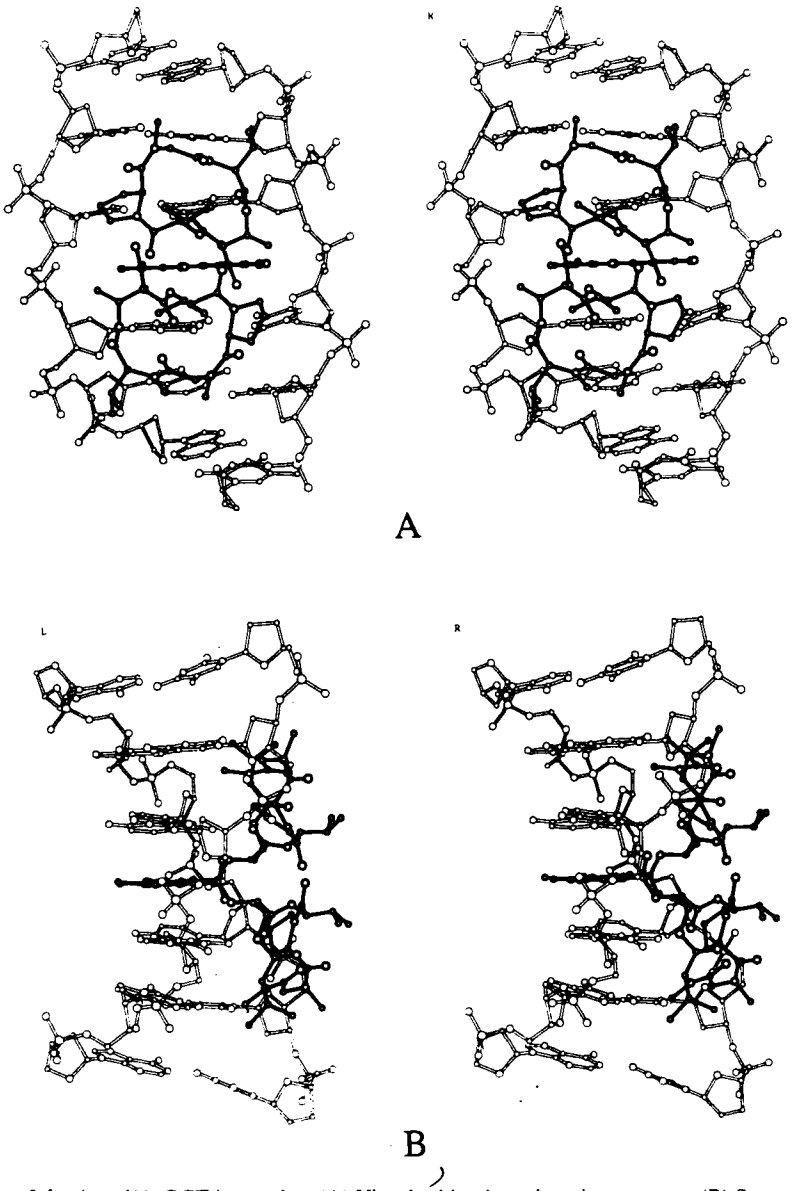

Fig. 7. Stereoviews of the Act–d(A_3GCT_3) complex. (A) View looking into the minor groove. (B) Same view but rotated by 90° along the helix axis. The terminal A·T pairs at either end are deleted.

linkages at the Thr-Val, Sar-meVal, meVal-Thr and phenoxazone-Thr steps and *cis* peptide linkages at the Val-Pro and Pro-Sar steps observed in the crystalline state of free Act (Ginell et al., 1988) are retained in the Act–d(A_3GCT_3) complex in solution.

There is a distinct orientational pattern of the polar functional groups of Act in relation to whether they are directed either towards or away from the DNA. The carbonyl groups of the Pro-Sar, Sar-meVal and meVal-Thr linkages are approximately normal to the helix axis and directed towards solvent away from the DNA minor groove in the complex. The carbonyl group

TABLE 5
TORSION ANGLES FOR LINKAGE BETWEEN PHENOXAZONE AND CYCLIC PENTAPEPTIDE RINGS FOR THE Act–d(A_3GCT_3) COMPLEX IN SOLUTION COMPARED TO VALUES FOR FREE Act IN THE CRYSTAL

Atom designation	Act–d(A_3GCT_3)		Act[a]
	Quinonoid	Benzenoid	
C(P2)-C(P1)-C(P17)-N(1)	110	100	131 ± 19
C(P1)-C(P17)-N(1)-C$^{\alpha}$(1)	177	181	182 ± 5
C(P17)-N(1)-C$^{\alpha}$(1)-C(1)	215	227	215 ± 7

[a] These values represent an average of the six Act conformations observed in the crystalline state (Ginell et al., 1988).

of the Val-Pro linkage is aligned along the helix axis and directed towards the other cyclic peptide and participates in Val(CO)-Val(NH) hydrogen-bond formation (length 1.43 Å and angle 167°). The carbonyl group of Thr is inclined away from the helix axis towards the DNA and can serve as an intermolecular hydrogen bond acceptor in the complex. The amide proton of Thr is directed towards the DNA and can serve as an intermolecular hydrogen-bond donor in the complex.

The hydrophobic methyl and methylene functionalities on the cyclic pentapeptide rings are distributed between those that are directed away and those that are directed towards the DNA. The CH_3 side chains of Val and meVal, as well as the NCH_3 group of Sar are directed towards the exterior away from the DNA while the NCH_3 group of meVal and the $C^{\alpha}H_2$ protons of Sar are directed towards the floor of the minor groove of the complex. The Pro ring protons and the CH_3 group of Thr are directed towards the sugar-phosphate backbone in the complex.

DNA conformation in complex

A qualitative examination of the experimental NOE data on the Act–d(A_3GCT_3) complex in H_2O and D_2O established that the non-terminal A·T and G·C base pairs adopt Watson-Crick alignments, the glycosidic torsion angles are in the *anti* range and the sugar puckers are in the C2′-*endo* range and the helix retains its right-handed pitch. These features are an integral part of the NMR-MD solution structure of the Act–d(A_3GCT_3) complex. The glycosidic torsion angles and sugar pucker pseudorotation angles for the central $(A3\text{-}G4\text{-}C5\text{-}T6)_I$·$(A3\text{-}G4\text{-}C5\text{-}T6)_{II}$ in the Act–d(A_3GCT_3) complex are listed in Table 6.

Geometry at the intercalation site

The alignment of the phenoxazone chromophore and the overlap geometry with respect to the flanking G·C base pairs in the NMR-MD refined structure reflect the intermolecular NOEs observed experimentally between the phenoxazone and nucleic acid residues defining the intercalation site. The long axis of the phenoxazone is aligned colinearly with the long axis of the flanking G·C base pairs with the quinonoid edge directed towards the $G4_I$-$C5_I$ backbone and the benzenoid edge directed towards the $G4_{II}$-$C5_{II}$ backbone in the complex (Fig. 8). The quinonoid NH_2 protons at the 2-position on the phenoxazone ring form a weak intermolecular hydrogen bond (length 2.09 Å and angle 145°) with the O3′ phosphate oxygen in the $(G4\text{-}C5)_I$ step in the complex.

TABLE 6
SELECTIVE HELICAL PARAMETERS[a] IN THE NMR-MOLECULAR DYNAMICS REFINED STRUCTURE OF THE Act–d(A_3GCT_3) COMPLEX

	χ^b	P[c] (Pucker)
Strand I		
A3	−88	147 (C2′-*endo*)
G4	−100	126 (C1′-*exo*)
C5	−93	187 (C3′-*exo*)
T6	−146	180 (C2′-*endo*)
Strand II		
A3	−88	147 (C2′-*endo*)
G4	−91	108 (C1′-*exo*)
C5	−102	138 (C1′-*exo*)
T6	−106	179 (C2′-*endo*)

[a] Derived using the CURVE programs.
[b] Glycosidic torsion angle.
[c] Sugar pucker pseudorotation angle.

The phenoxazone ring sits centrally in the intercalation cavity (Fig. 8A shows only the backbone atoms and hence does not include the H7 and H8 protons on the benzenoid edge) and overlaps with the guanosine but not cytosine bases of flanking G·C base pairs (Fig. 8B). Indeed, there is no overlap between guanosine and cytosine bases in G-C steps at the phenoxazone intercalation site (Fig. 8B), in contrast to significant overlap at such steps in crystal structures of free DNA oligomer duplexes (Dickerson and Drew, 1981).

We note that the G4·C5 base pairs flanking the phenoxazone intercalation site are parallel to each other (Fig. 8A) with the increased separation between these base pairs reflected in the inter-proton separation between the base proton of C5 and the sugar H1′ and H3′ protons of G4 in the complex. The formation of the Act intercalation site is accompanied by a small overwinding between the central G4·C5 base pairs such that the helical twist is 39° at this site in the complex. By contrast, a pronounced unwinding is observed between the A3·T6 and G4·C5 base pairs such that the helical twist is 17.5° at these steps on either side of the intercalation site. Further, the minor groove widens at the Act binding site such that the cross-strand P-P separation is 16.4 Å at the intercalation site and 18.2 Å between A3-G4 and C5-T6 phosphates on partner strands in the complex.

Intermolecular contacts in the minor groove

We observe a complementary fit between the cyclic pentapeptides of actinomycin and the minor groove on either side of the intercalation site in the Act–d(A_3GCT_3) complex.

A set of intermolecular hydrogen bonds account for the sequence specificity of actinomycin for (G-C)·(G-C) sites on duplex DNA. The NH_2-2 group of G4 forms a strong intermolecular hydrogen bond with the carbonyl of Thr (distance 1.44 Å and angle 128°) while the N3 of G4 forms a

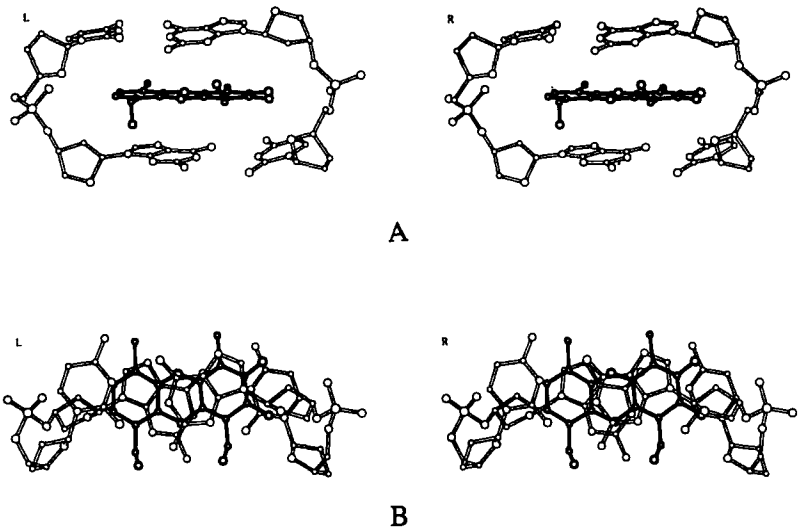

Fig. 8. Stereoviews of the intercalation site (drug phenoxazone chromophore and adjacent G·C pairs) in the Act–$d(A_3GCT_3)$ complex. (A) This view emphasizes the parallel alignment of the base pairs flanking the intercalation site. (B) This view emphasizes the overlap geometry between the phenoxazone ring and flanking base pairs.

weak intermolecular hydrogen bond with the amide proton of Thr (distance 1.90 Å and angle 131°) in the NMR-MD refined structure of the Act–$d(A_3GCT_3)$ complex.

Several van der Waals contacts between the complementary surfaces of the cyclic pentapeptide and the DNA minor groove stabilize formation of the Act–$d(A_3GCT_3)$ complex. These include intermolecular interactions between the ring protons of Pro and the C5 sugar, between the Hα of meVal and the G4 sugar and between the geminal H^{α} protons of Sar and the NCH_3 protons of meVal and the minor groove edge of the A3·T6 base pair (Table 3 and Fig. 7).

DISCUSSION

'Sobell and Jain' model of the Act–DNA complex

A detailed molecular model has been proposed for the Act–d(ATGCAT) complex (Sobell and Jain, 1972; Sobell, 1973) based on the single crystal X-ray structure of the Act-dG (1 drug per 2 nucleosides) complex (Sobell et al., 1971; Jain and Sobell, 1972). The key features of this model are the following. (1) The phenoxazone ring of Act intercalates at (G-C)·(G-C) steps on duplex DNA with the cyclic pentapeptide rings lying in the minor groove. (2) The sequence specificity of Act for G-C steps on duplex DNA is associated with intermolecular hydrogen-bond formation between the N3 and NH_2-2 groups along the minor groove edge of guanosine and the NH and CO groups of Thr on the drug, respectively. (3) Each cyclic pentapeptide ring spans two base pairs on either side of the intercalated phenoxazone chromophore with the complex stabilized by hydrophobic interactions between the cyclic pentapeptide rings and the minor groove of the DNA. (4) The sugar pucker is postulated to be G(C3'-*endo*)-C(C2'-*endo*) at the intercalation site. (5) The helix unwinding is postulated to be $-18°$ between G3·C4 base pairs at the intercalation site and $-8°$ between G3·C4 and T2·A5 base pairs proximal to the intercalation site in opposite directions.

This corresponds to a total unwinding of $-34°$ [$-18° + 2(-8°)$] over the four central base pairs in the Act–d(A1-T2-G3-C4-A5-T6) complex. (6) The symmetry axis relating the two cyclic pentapeptide rings coincides with the symmetry axis relating the DNA base and sugar-phosphate backbone.

Clearly, there are assumptions associated with deriving an intercalative model of the Act–d(ATGCAT) complex (Sobell and Jain, 1972; Sobell, 1973) based on an X-ray structure of a stacked Act–dG complex (1 drug per 2 nucleosides). A more appropriate starting point would be an X-ray structure of a miniature intercalative complex such as Act–d(G-C) (1 drug per 2 dinucleotides). Such a complex has been crystallized with the surprising result that the d(G-C) dinucleotide is in an extended conformation and an intercalative complex does not form (Takusagawa et al., 1982). The Act–d(G-C) complex is interesting, however, since G·C base pairs do stack on either side of the phenoxazone chromophore and provide insights into stacking interactions. The critical X-ray data in support of an intercalative model of the Act–DNA complex is not at hand and all attempts to crystallize and solve such a structure have been unsuccessful to date. There is therefore a need to evaluate the major structural conclusions by direct studies of Act–DNA oligomer complexes by NMR in aqueous solution.

Previous NMR research on Act–DNA oligomer complexes

The Act–d(ATGCAT) complex (1 drug per duplex) has been investigated by both one-dimensional (Patel, 1974b) and two-dimensional (Brown et al., 1984) NMR studies in aqueous solution. The former NMR study established that Act intercalated at the G-C step in the d(ATGCAT) duplex without disruption of the flanking G·C pairs (Patel, 1974b). The latter NMR study (Brown et al., 1984) was combined with molecular dynamics computations (Creighton et al., 1989) to propose a solution conformation of the complex. There were substantial differences between interproton distances in the computed structure of the complex and input constraints provided by the NMR data set. This reflects serious limitations in the accuracy of the NMR-derived distance constraints since the analysis was based on a single long 200 ms mixing time NOESY data set (Brown et al., 1984). Spin diffusion will clearly invalidate the two-spin approximation used to estimate the interproton distances in the complex.

The Act–d(AGCT) complex (1 drug per duplex) was independently investigated by one-dimensional (Reid et al., 1983) and two-dimensional (Delepierre et al., 1989) NMR studies in aqueous solution. The contribution by Reid et al. (1983), was especially timely since they were the first to assign critical intermolecular NOEs that established both intercalation of the phenoxazone ring and positioning of the cyclic pentapeptide rings in the minor groove. The two-dimensional NMR study of this complex by Delepierre et al. (1989) included assignment of the nucleic acid and drug protons, as well as measurement of coupling constants (^1H-^1H and ^1H-^{31}P) and estimation of distance constraints (based on short mixing time NOESY data sets and defined by loose bounds). The distance constraints were coupled with molecular mechanics refinement to deduce structural features of the solution conformation of the Act–d(AGCT) complex (Delepierre et al., 1989). This paper emphasized the NMR aspects of the problem and little information was provided on the number and types of intermolecular constraints and the extent of agreement between experimental and calculated interproton distances in the complex. It also appears that different starting structures were not sampled and the analysis may be limited to local searches of conformational space by the molecular mechanics algorithm.

Our study on the Act–d(A_3GCT_3) complex (1 drug per duplex) was undertaken in the context of parallel studies being conducted in our laboratory on the Act–d(A_2GCGCT_2) complex (2 drugs per duplex). Wilson and co-workers have previously established that two Act molecules can intercalate at adjacent G-C steps in a G-C-G-C segment (Wilson et al., 1986; Jones et al., 1988; Scott et al., 1988a,b). It was clear that two equivalents of Act form an unusual complex with the G-C-G-C duplex segment since a structural rearrangement is mandatory to relieve potential steric clashes between inwardly pointing cyclic pentapeptide rings of adjacently bound Act molecules where the intercalation sites are separated by only two base pairs. Thus, our NMR structural studies on the Act–d(A_3GCT_3) complex reported in this study would serve as the normal control for related studies on the unusual Act–d(A_2GCGCT_2) complex.

The Act–d(A_3GCT_3) complex project is also of intrinsic interest since there is no X-ray structure of an intercalation Act–DNA oligomer complex (1 drug per duplex). The key concepts to emerge from our NMR-MD study of the Act–d(A_3GCT_3) complex are discussed below.

Act conformation in crystallographic and solution complexes

The same conformation has been observed for Act in the X-ray structures of the free antitumor drug (Ginell et al., 1988) and its complexes with dG (Sobell et al., 1971; Jain and Sobell, 1972) and d(G-C) (Takusagawa et al., 1982). The observed pattern of *trans* and *cis* peptide/ester linkages fixes the orientation of the cyclic pentapeptide rings. Further, the NH(Val) to CO(Val) hydrogen bonds between cyclic pentapeptide rings define and fix their relative alignment. The structure of the Act in the d(A_3GCT_3) complex in solution is similar to that observed in the crystalline state except for a crank-shaft motion at the backbone torsion angles flanking the meVal-Thr ester linkage (see differences for the $O^{\beta}(1)$-C(5) torsion angle of meVal and the $C^{\beta}(1)$-$O^{\beta}(1)$ torsion angle of Thr in Table 4). Thus, the ester group linking meVal and Thr is oriented parallel to the long axis of the phenoxazone in the crystal of the free drug but is oriented orthogonal to the long axis of the phenoxazone and pointing towards the exterior in the Act–d(A_3GCT_3) complex. This transition is necessary to avoid a steric clash between the ester carbonyl and the DNA backbone on complex formation.

There are three torsion angles that link the phenoxazone ring with the benzenoid and quinonoid cyclic pentapeptide rings of Act. We note that these torsion angles about the C(P1)-C(P17), C(P17)-N(1) amide and N(1)-C^{α}(1) bonds (see Table 5 for nomenclature) in the Act–d(A_3GCT_3) complex in solution are similar to the values for free Act in the crystalline state (Table 5). Thus the overall right-handed structural domain formed by the relative alignment of the benzenoid and quinonoid cyclic pentapeptide rings of Act observed in crystallographic studies (Sobell et al., 1971; Takusagawa et al., 1982; Ginell et al., 1988) are retained in the structure of the Act–d(A_3GCT_3) complex in solution.

Polar and nonpolar functional groups are observed on the faces of the cyclic pentapeptides that are directed towards and away from the DNA in the Act–d(A_3GCT_3) complex. Of special importance is the alignment of the NH and CO groups of Thr on the benzenoid and quinonoid cyclic pentapeptide rings which are symmetrically positioned on either side of the phenoxazone chromophore. These polar functionalities are oriented towards the DNA and form symmetry-related pairs of intermolecular hydrogen bonds with the minor groove edge of guanosines in the (G-C)·(G-C) intercalation site step.

$(A3\text{-}G4\text{-}C5\text{–}T6)_I$·$(A3\text{-}G4\text{-}C5\text{-}T6)_{II}$ segment in solution complex

The observed directionality of NOE connectivities between base and adjacent sugar protons (Fig. 2) is consistent with formation of a right-handed helix for the $(A3\text{-}G4\text{-}C5\text{-}T6)_I$·$(A3\text{-}G4\text{-}C5\text{-}T6)_{II}$ segment in the Act–d(A_3GCT_3) complex.

The observed NOEs between the imino proton of G4 and the hydrogen-bonded and the exposed amino protons of C5 (Fig. 1) establish that both $G4_I$·$C5_{II}$ and $G4_{II}$·$C5_I$ pair through Watson-Crick alignment at the intercalation site in the Act–d(A_3GCT_3) complex. Similarly, the observed NOEs between the imino protons of T6 and the H2 proton of A3 establish formation of Watson-Crick A3·T6 pairs one step removed from the intercalation site.

The sugars at the intercalation site adopt a G4(C1′-*exo*)-C5(C3′-*exo*/C1′-*exo*) pucker in the structure of the Act–d(A_3GCT_3) complex (Table 6). Both puckers are in the C2′-*endo* range and we have not found evidence supporting the mixed G(C3′-*endo*)-C(C2′-*endo*) pucker proposed in the Sobell and Jain (1972) model of the Act–DNA complex. It should also be noted that the sugar puckers of A3 and T6 which are one base pair removed from the intercalation site also retain a C2′-*endo* sugar pucker in the Act–d(A_3GCT_3) complex (Table 6). The glycosidic torsion angles for G4 and C5 at the intercalation site adopt values in the $-95 \pm 5°$ range in the Act–d(A_3GCT_3) complex (Table 6). These glycosidic torsion angles in the complex are in the high *anti* range and characteristic of B-DNA ($-95°$) rather than A-DNA ($-153°$) values.

The NMR distance constraints of nucleic acid protons are restricted to the base and sugar protons on the same and adjacent residues and under the best of circumstances provide structural information primarily on helical parameters such as glycosidic torsion angles, sugar puckers and the twist angle between adjacent base pair steps (Metzler et al., 1990). The available NMR data do not provide estimates of the torsion angles in the sugar-phosphate backbone and the molecular dynamics must reflect one low-energy solution to the conformation of the backbone linkage connecting adjacent sugar residues in the Act–d(A_3GCT_3) complex.

Intercalation site in the Sobell-Jain model and solution complex

The Act–d(A_3GCT_3) complex is stabilized by extensive overlap between the phenoxazone ring and the flanking G·C base pairs at the intercalation site. This overlap presented in Fig. 8B is very similar to that observed between the phenoxazone ring and flanking G·C base pairs in the X-ray structure of the non-intercalative Act–d(G-C) complex (1 drug per 2 dinucleotides) (Takusagawa et al., 1982). The phenoxazone ring stacks extensively with flanking guanosines but not at all with flanking cytidines in both the present study of the Act–d(A_3GCT_3) complex and the X-ray study of the Act–d(G-C) complex.

The structure of the Act–d(A_3GCT_3) complex exhibits an overwinding of $+3°$ at the intercalative site step and an unwinding of $-18.5°$ at the next base pair steps in either direction away from the intercalation site. This corresponds to a total unwinding of $-34°$ [$3° + 2(-18.5°)$] spread over four base pairs centered about the intercalation site. This conclusion that there is no unwinding at the intercalation step but pronounced unwinding at the next base pair steps in either direction in the Act–d(A_3GCT_3) complex differs from the Sobell-Jain model which proposed the most pronounced unwinding at the intercalation step. It should be noted that in the X-ray structure of the daunomycin–DNA oligomer complex, no unwinding is observed at the aglycone intercalation site but instead an unwinding of $-8°$ is observed at the next base pairs in either direction from the intercalation site (Wang et al., 1987).

Minor groove recognition and stabilization by bound Act in the solution complex

The observation of separate hydrogen-bonded and exposed amino protons of $G4_I$ and $G4_{II}$ (Fig. 1) provides markers at the minor groove edge of the $(G4\text{-}C5)_I \cdot (G4\text{-}C5)_{II}$ intercalation site in the Act–$d(A_3GCT_3)$ complex. The data are consistent with the exposed amino proton of G4 participating in an intermolecular hydrogen bond with an acceptor group on the bound Act. Indeed, two symmetry-related strong hydrogen bonds are formed between the exposed NH_2 proton of G4 and the carbonyl group of Thr in the Act–$d(A_3GCT_3)$ complex. This intermolecular hydrogen bond is an important prediction of the Sobell-Jain (1972) model of the Act–DNA complex and our results support this proposal. It is important to stress that no intermolecular hydrogen bonding constraints were included in the molecular dynamics computations of the Act–$d(A_3GCT_3)$ complex.

The exposed NH_2 protons of G4 exhibit NOEs to the amide protons of Thr and the NCH_3 protons of meVal (Table 3) and help to position the Act in the minor groove of the $d(A_3GCT_3)$ duplex.

Complementarity of peptide-nucleotide surfaces in complex

Color views of CPK models of the structure of the Act–$d(A_3GCT_3)$ complex are shown in Fig. 9 with the left panel looking into the major groove, the central panel emphasizing the intermolecular drug cyclic pentapeptide-DNA backbone contacts and the right panel looking into the minor groove. These space-filling models emphasize the complementarity of the fit between the Act and the DNA on complex formation.

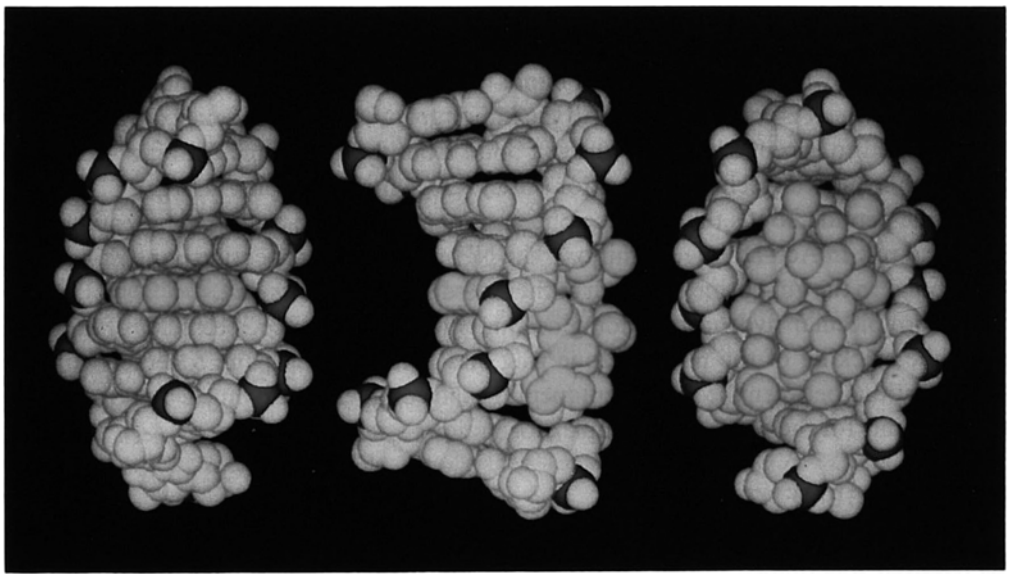

Fig. 9. Space-filling views of the Act–$d(A_3GCT_3)$ complex in solution. (Left) View looking into the major groove. (Middle) View emphasizes the complementary fit between the cyclic pentapeptide backbone of Act and the sugar-phosphate backbone in the minor groove. (Right) View looking into the minor groove. Note the excellent fit between the two cyclic pentapeptide rings and the walls of the expanded minor groove.

The cyclic pentapeptide lactone rings of Act adopt a rigid rectangular shape primarily determined by the distribution of *trans* peptide (Sar-meVal, Thr-Val and phenoxazone-Thr), *trans* ester (meVal-Thr) and *cis* peptide (Val-Pro and Pro-Sar) linkages. We discuss below the intermolecular interactions between each side of the rectangular cyclic pentapeptide rings of Act and the complementary surface on the $(A3\text{-}G4\text{-}C5\text{-}T6)_I \cdot (A3\text{-}G4\text{-}C5\text{-}T6)_{II}$ segment of the $d(A_3GCT_3)$ duplex.

One short side of the rectangular cyclic pentapeptide starts at the nitrogen atom of Pro and ends at the nitrogen atom of adjacent Sar. This backbone segment is parallel to the DNA backbone extending from the C5 sugar to the T6 sugar. A set of intermolecular contacts between the ring protons of Pro and the sugar protons of C5 and between the NCH_3 protons of Sar and the sugar protons of T6 (Table 3) establishes the complementary van der Waals interactions between this peptide segment and one of the DNA strands in the Act–$d(A_3GCT_3)$ complex.

The next side proceeding around the rectangular cyclic pentapeptide starts at the nitrogen atom of Sar and extends to the Cα atom of adjacent meVal. A hydrophobic patch including the methylene protons of Sar and the NCH_3 protons of meVal is directed towards the minor groove base pair edge of the A3·T6 base pair (Table 3). The methylene protons of Sar are closer to the T6 sugar on one strand while the NCH_3 group of meVal is closer to the G4 sugar on the other strand (Table 3) so that this peptide segment effectively interacts through van der Waals contacts with the bases and sugars on both strands.

This is followed by another short peptide segment extending from the C^α of meVal to the C^α of Thr which is parallel to the DNA backbone between adjacent phosphates that link the G4 residue. The H^α of meVal and the CH_3 protons of Thr are directed towards the sugar of G4 (Table 3) and interact with one of the DNA strands in the complex.

The remaining peptide segment extends from the C^α atom of Thr to the N atom of Pro. None of the protons in this cyclic pentapeptide segment is directed towards the DNA. Rather, the NH and CO groups of Thr are parallel to the helix axis and participate in hydrogen bonds between the cyclic pentapeptide rings. These hydrogen bonds align the cyclic pentapeptide rings into a right-handed domain which is complementary to the minor groove of the DNA helix. The CO group of Thr is positioned to accept a strong hydrogen bond from the guanosine 2-amino group which is critical for the sequence specificity of Act for (G-C)·(G-C) sites on duplex DNA.

Finally, the peptide bonds that link the phenoxazone ring to the cyclic pentapeptide rings also play a critical role in Act–DNA recognition. The NH proton of this peptide bond donates a weak hydrogen bond to the guanosine N3 atom in the Act–$d(A_3GCT_3)$ complex.

Thus, intermolecular hydrogen bonding accounts for the sequence specificity of complex formation while stacking of the phenoxazone ring and flanking G·C pairs together with van der Waals interactions between the cyclic pentapeptide and complementary nucleic acid minor groove surfaces accounts for the stability of complex formation.

ACKNOWLEDGEMENTS

This research was funded in part by Columbia University start-up funds and in part by NIH CA-46778. The NMR spectrometers were purchased from funds donated by the Robert Woods Johnson Jr. Trust and Matheson Trust towards setting up the NMR Center in the Basic Medical Sciences at Columbia University. The 600 MHz NMR data were collected at the National NMR Facility at Madison, Wisconsin, supported by NIH Grant RR-02301.

REFERENCES

Brown, S.C., Shafer, R.H. and Mirau, P.A. (1982) *J. Am. Chem. Soc.*, **104**, 5504–5506.

Brown, S.C., Mullis, K., Levenson, C. and Shafer, R.H. (1984) *Biochemistry*, **23**, 403–408.

Cerami, A., Reich, E., Ward, D.C. and Goldberg, I.H. (1967) *Proc. Natl. Acad. Sci. U.S.A.*, **57**, 1036–1042.

Creighton, S., Rudolph, B., Lybrand, T., Singh, U.C., Shafer, R., Brown, S., Kollman, P., Case, D.A. and Andrea, T. (1989) *J. Biomol. Struct. Dyn.*, **6**, 929–969.

Delepierre, M., van Heijenoort, C., Igolen, J., Pothier, J., LeBret, M. and Roques, B.P. (1989) *J. Biomol. Struct. Dyn.*, **7**, 557–589.

Dickerson, R.E. and Drew, H.R. (1981) *J. Mol. Biol.*, **149**, 761–786.

Fox, K.R. and Waring, M.J. (1984) *Nucl. Acids Res.*, **12**, 9271–9285.

Gao, X. and Patel, D.J. (1988) *Biochemistry*, **27**, 1744–1751.

Gao, X. and Patel, D.J. (1989) *Biochemistry*, **28**, 751–762.

Gao, X., Mirau, P. and Patel, D.J. (1991) *J. Mol. Biol.*, in press.

Ginell, S., Lessinger, L. and Berman, H.M. (1988) *Biopolymers*, **27**, 843–864.

Jain, S.C. and Sobell, H.M. (1972) *J. Mol. Biol.*, **68**, 1–20.

Jones, R.L., Scott, E.V., Zon, G., Marzilli, L.G. and Wilson, W.D. (1988) *Biochemistry*, **27**, 6021–6026.

Krugh, T.R. (1972) *Proc. Natl. Acad. Sci. U.S.A.*, **69**, 1911–1914.

Krugh, T.R. and Chen, Y.C. (1975) *Biochemistry*, **14**, 4912–4922.

Krugh, T.R. and Neely, J.W. (1973) *Biochemistry*, **12**, 4418–4425.

Metzler, W.J., Wang, C., Kitchen, D., Levy, R.M. and Pardi, A. (1990) *J. Mol. Biol.*, **214**, 711–736.

Muller, W. and Crothers, D.M. (1968) *J. Mol. Biol.*, **35**, 251–290.

Patel, D.J. (1974a) *Biochemistry*, **13**, 2388–2396.

Patel, D.J. (1974b) *Biochemistry*, **13**, 2396–2402.

Patel, D.J. (1976a) *Biochem. Biophys. Acta*, **442**, 98–108.

Patel, D.J. (1976b) *Biopolymers*, **15**, 533–558.

Patel, D.J. and Canuel, L.L. (1977) *Proc. Natl. Acad. Sci. U.S.A.*, **74**, 2624–2628.

Patel, D.J., Kozlowski, S.A., Rice, J.A., Broka, C. and Itakura, K. (1981) *Proc. Natl. Acad. Sci. U.S.A.*, **78**, 7281–7284.

Petersheim, M., Mehdi, S. and Gerlt, J.A. (1984) *J. Am. Chem. Soc.*, **106**, 439–440.

Reich, E. and Goldberg, I.H. (1964) *Progress in Nucleic Acids Research and Molecular Biology* **3**, 183–234.

Reid, D.G., Salisbury, S.A. and Williams, D.H. (1983) *Biochemistry*, **22**, 1377–1385.

Scott, E.V., Jones, R.L., Banville, D.L., Zon, G., Marzilli, L.G. and Wilson, W.D. (1988a) *Biochemistry*, **27**, 915–923.

Scott, E.V., Zon, G., Marzilli, L.G. and Wilson, W.D. (1988b) *Biochemistry*, **27**, 7940–7951.

Sobell, H.M. (1973) *Progress in Nucleic Acids Research and Molecular Biology*, **13**, 153–190.

Sobell, H.M. and Jain, S.C. (1972) *J. Mol. Biol.*, **68**, 21–34.

Sobell, H.M., Jain, S.C. and Sakore, T.D. (1971) *Nature New Biology*, **231**, 200–205.

Takusagawa, F., Dabrow, M., Neidle, S. and Berman, H.M. (1982) *Nature*, **296**, 466–469.

Van de Ven, F.J. and Hilbers, C.W. (1988) *Eur. J. Biochem.*, **178**, 1–38.

Van Dyke, M.W., Hertzberg, R.P. and Dervan, P.B. (1982) *Proc. Natl. Acad. Sci. U.S.A.*, **79**, 5470–5474.

Wang, A.H., Ughetto, G., Quigley, G. and Rich, A. (1987) *Biochemistry*, **26**, 1152–1163.

Waring, M. (1970) *J. Mol. Biol.*, **54**, 247–279.

Waring, M. (1981) In *The Molecular Basis of Antibiotic Action* (Eds, Gale, F. et al.) Wiley, London, pp. 314–333.

Wells, R.D. and Larson, J.E. (1970) *J. Mol. Biol.*, **49**, 319–342.

Wilson, W.D., Jones, R.L., Zon, G., Scott, E.V., Banville, D.M. and Marzilli, L.G. (1986) *J. Am. Chem. Soc.*, **108**, 7113–7114.

Wüthrich, K. (1986) *NMR of Proteins and Nucleic Acids*, Wiley, New York.

Zhang, X. and Patel, D.J. (1990) *Biochemistry*, **29**, 9451–9466.

Zhang, X. and Patel, D.J. (1991) *Biochemistry*, **30**, 4026–4041.